

Double-slit implementation of minimal Deutsch algorithm

B. Marques¹, M. R. Barros¹, W. M. Pimenta¹, M. A. D. Carvalho¹,
J. Ferraz¹, R. C. Drumond^{1,2,3}, M. Terra Cunha³, and S. Pádua¹

¹*Departamento de Física, Universidade Federal de Minas Gerais,
caixa postal 702, 30123-970, Belo Horizonte, MG - Brazil*

²*Instituto Nacional de Matemática Pura e Aplicada IMPA Estrada Dona Castorina,
110 Jardim Botânico 22460-320, Rio de Janeiro, RJ, Brazil and*

³*Departamento de Matemática, Universidade Federal de Minas Gerais,
caixa postal 702, 30161-970, Belo Horizonte, MG - Brazil*

We report an experimental implementation of the minimal Deutsch algorithm in an optical setting. In this version, a redundancy is removed from the most famous form of the algorithm. The original version involves manipulation of two qubits, while in its minimal version, only one qubit is used. Our qubit is encoded in the transversal spatial modes of a spontaneous parametric down-converted signal photon, with the aid of a double slit, with the idler photon playing a crucial role in creating a heralded single photon source. A spatial light modulator (SLM) is programmed to physically generate one-bit functions necessary to implement the algorithm's minimal version, which shows that the SLM can be used in future implementations of quantum protocols.

I. INTRODUCTION

Quantum computation has emerged in the past decades as a potentially powerful tool to solve problems more efficiently than its classical counterpart. One simple example is determining whether a coin is fair (heads on one side, tails on the other) or fake (heads or tails on both sides). This is one version of *the Deutsch problem* [1], who himself showed that, when exploring quantum state superposition, only one examination step is necessary, while classically the solution requires individual examination of both sides. Although the algorithm originally proposed by Deutsch involves manipulation of two-qubit states, there is also a “minimal” version of it, in the sense that just one qubit is manipulated [2]. In this sense, minimal Deutsch algorithm can be considered the most basic and simple quantum computation.

Many physical systems have shown to be useful for implementing quantum computation, such as nuclear magnetic resonance [3, 4], trapped ions [5], optical cavities [6], Josephson junctions [7], and photons [8, 9]. In particular, the original Deutsch algorithm and its generalization, the Deutsch-Jozsa algorithm [10], were implemented using photons [9, 11], and its minimal version was also implemented on quantum dots [12].

Spontaneous parametric down conversion (SPDC) [13] is a natural source of correlated photon pairs, with the additional advantage of having many degrees of freedom that can be considered quantum systems, such as polarization [13, 14], transversal [15], longitudinal [16, 17], and orbital angular [18, 19] momenta. On the other hand, a spatial light modulator (SLM) can be used to perform state control [20]. It has been used for tomographing polarization [21] and transverse momenta [22] states, for measuring Bell inequality violations in orbital momenta of SPDC photon pairs [23], and optical quantum algorithm simulation [24].

In this work we report an experimental implementa-

tion of the minimal Deutsch algorithm in an optical setting. We use a double slit to encode logical qubits (in the sense of the $\{|0\rangle, |1\rangle\}$ logical base of a qubit space) in the transversal spatial modes of photons generated in a SPDC process [15]. A SLM is employed as a fundamental part of our experimental setup. It has the function of simulating the “fair coin” or the “fake coin” in the optical setup. Before really applying the quantum algorithm, we need a calibration process, which can also be understood as a proof of principle of the algorithm, since one uses many carries of the oracle. After such calibration, the apparatus is ready for running the real Deutsch algorithm: With only one “examination step”, answer which type of “coin” we have, with probability larger than $1/2$. The paper is organized as follows: In Sec. II we review the theoretical description of the minimal Deutsch algorithm. The experimental setup is presented in Sec. III. The results are shown in Sec. IV. Discussion is made in Sec. V and conclusions are outlined in Sec. VI.

II. MINIMAL DEUTSCH ALGORITHM

Quantum parallelism allows quantum systems to evaluate a function $f(x)$ for many different values of x simultaneously. The Deutsch algorithm is a good example of how to explore quantum parallelism to answer a classical question; explicitly, to solve the Deutsch problem evaluating the function only once.

Consider an *oracle* that can answer one-bit questions with one bit answers described by a deterministic function $f : \{0, 1\} \rightarrow \{0, 1\}$. This function is called balanced if $f(0) \neq f(1)$, otherwise the function is constant [$f(0) = f(1)$]. The Deutsch problem consists in determining whether a given unknown function is balanced or constant. For a classical algorithm to answer that with certainty it requires the oracle to be asked twice, that is, asking the value of f on 0 and 1. On the other hand, the Deutsch algorithm requires only a single query, us-

ing quantum parallelism, to reduce the minimal resource required.

In the minimal version [2], the oracle's behavior is encoded in a unitary operation U_f to be applied on a well-chosen input state, depending on the function f . For the computational basis one has $U_f |x\rangle = (-1)^{f(x)} |x\rangle$ as output, for $x = 0, 1$. Now, if the superposition state $\frac{1}{\sqrt{2}}(|0\rangle + |1\rangle)$ is used as input, both questions are asked at the same time, with the output state being:

$$|\psi\rangle = U_f \frac{|0\rangle + |1\rangle}{\sqrt{2}} = \frac{(-1)^{f(0)} |0\rangle + (-1)^{f(1)} |1\rangle}{\sqrt{2}}. \quad (1)$$

Disregarding global phases, one has:

$$|\psi\rangle = \begin{cases} |+\rangle = \frac{1}{\sqrt{2}}(|0\rangle + |1\rangle), & \text{if } f(0) = f(1), \\ |-\rangle = \frac{1}{\sqrt{2}}(|0\rangle - |1\rangle), & \text{if } f(0) \neq f(1). \end{cases} \quad (2)$$

Note that the first answer is orthogonal to the second, so we can make a projective measurement in the basis $\{|+\rangle, |-\rangle\}$ and find out if the function is balanced ($|-\rangle$) or constant ($|+\rangle$). The unitary operations are implemented by the oracle. Four possible maps U_{ij} are generated and we label them with the values of $i = f(0)$ and $j = f(1)$:

$$\begin{aligned} U_{00} &= \begin{bmatrix} 1 & 0 \\ 0 & 1 \end{bmatrix} & f(0) = f(1) = 0, \\ U_{01} &= \begin{bmatrix} 1 & 0 \\ 0 & -1 \end{bmatrix} & f(0) = 0 \neq f(1) = 1, \\ U_{10} &= \begin{bmatrix} -1 & 0 \\ 0 & 1 \end{bmatrix} & f(0) = 1 \neq f(1) = 0, \\ U_{11} &= \begin{bmatrix} -1 & 0 \\ 0 & -1 \end{bmatrix} & f(0) = f(1) = 1. \end{aligned} \quad (3)$$

III. EXPERIMENTAL SETUP

The scheme of the experimental setup is shown in Fig.1. A 50 mW He-Cd laser operating at $\lambda = 325$ nm is used to pump a 2-mm-thick lithium iodate crystal and generate, by type I SPDC, degenerate non-collinear photon pairs. Signal and idler ($\lambda_s = \lambda_i = 650$ nm) beams pass through a $\lambda/2$ plate (half-wave plate), before they cross a double-slit placed at a distance of 250 mm from the crystal. The double-slit plane (xy plane) is aligned perpendicular to the plane defined by the pump laser and the down-converted beams (yz plane), with the small dimension of the slits parallel to the x direction. The slits are $2a = 100$ μm wide and have a separation of $2d = 250$ μm . The lens L_1 is used to generate photon pairs in entangled transversal path states [25]. A natural question is why to use down-converted biphotons for implementing the one-qubit Deutsch algorithm. In our case, one can consider the selective detection of the idler photon as part of the heralded preparation of the signal photon state.

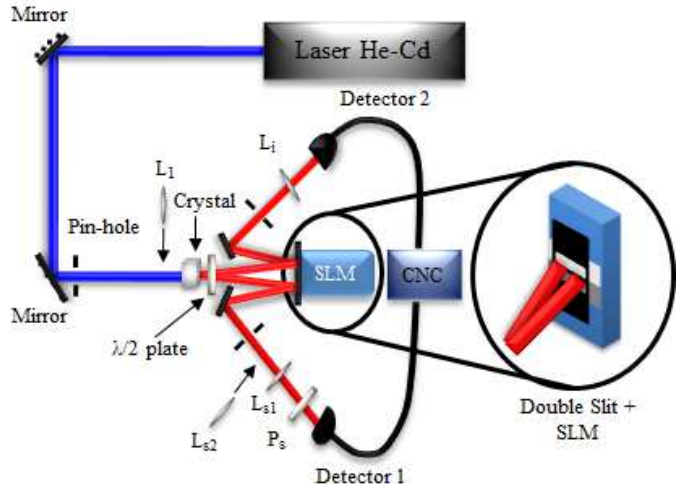


FIG. 1. (Color online) Experimental setup scheme for minimal Deutsch algorithm implementation. The L_1 lens focuses the pump beam in the double-slit plane; lenses L_{s1} and L_i are used to detect the signal and idler beams at Fourier plane, while the L_{s2} lens is used to project the double slit images in the detector. A half-wave plate is placed right after the crystal and a polarizer P_s is positioned in front of detector 1. CNC denotes coincidence counter and SLM denotes spatial light modulator.

Our experimental setup is arranged in a way that a photon passing through the inferior slit of the double slit corresponds to state $|0\rangle$, while a photon that passes through the superior slit corresponds to state $|1\rangle$. The SLM after the double slit, together with the $\lambda/2$ plate and the polarizer P_s , works as the quantum oracle. The map of the oracle function is constant (U_{00} or U_{11}) if the phases added by the SLM are equal, or balanced (U_{01} or U_{10}) if the phase difference is π . Once the pump beam is focused at the double slit plane, a Bell state $|\psi_+\rangle$ is created by the twin photons in the slit path states [25, 26]. A dichroic mirror placed just after the crystal removes the pump beam and transmits signal and idler beams. The trigger photon (idler) also passes through a double slit and is reflected by the SLM, but without the polarizer at its path, no phase change or amplitude variation in its state occurs due to the manner in which the SLM works. In Fig. 2 and Fig. 3, we show, experimentally, that we are able to introduce spatial phase changes at the signal-photon path state while preserving the state amplitudes by using the SLM. However, there are many other maps that the SLM can implement in a double slit-qubit. The SLM maps can be described by:

$$U_{SLM} = \begin{bmatrix} A_0 e^{i\phi_0} & 0 \\ 0 & A_1 e^{i\phi_1} \end{bmatrix}, \quad (4)$$

where A_k is the attenuation and ϕ_k is the phase applied in the photon state $|k\rangle$. The SLM maps in this kind of

setup are diagonal because it cannot exchange photon population between slits, i.e., an operation like $|0(1)\rangle \mapsto A_0|0\rangle + A_1|1\rangle$ cannot be done, if $A_k \neq 0$. Instances of these SLM maps were implemented in Refs. [21, 22], while a general one can be made through a calibration described by Moreno *et al.* [27].

Single slits with $100\ \mu\text{m}$ width are placed in front of each detectors. Their planes ($xy_{i,s}$ planes) are aligned perpendicular to the propagation direction of the idler and signal beams ($z_{i,s}$ direction), respectively. The small dimension of each slit is parallel to the corresponding x direction. The SLM used is a Holoeye Photonics LC-R 2500, which has a 1024×768 pixel resolution (each pixel consists of a $19 \times 19\ \mu\text{m}$ square) and it is controlled by a computer. Signal and idler beams are focused on the detectors with a microscope objective lens (not shown in Fig. 1). Two interference filters, centered at $650\ \text{nm}$ and $10\ \text{nm}$ FWHM bandwidth, are kept before the objective lenses. Pulses from the detectors are sent to a photon-counter and a coincidence detection setup with a $5.0\ \text{ns}$ resolving time.

IV. EXPERIMENTAL RESULTS

First of all, we must be able to implement the maps U_{ij} ($i, j \in \{0, 1\}$) of Eq. (3). It was shown [27] that a SLM plus the input and output polarizers can be properly calibrated to obtain this goal ($A_0 = A_1$ and $\phi_k = 0, \pi$). The liquid crystal display of the SLM is divided in two regions, each region adding a phase to the photon path state, $|0\rangle$ or $|1\rangle$, defined by the slits (inset of Fig. 1). A SLM gray level is associated with each region of the display. Pre-determined gray levels, along with correct half-wave plate and polarizer angles, introduce a relative phase between the photon path states without relative amplitude attenuation. The evolution maps U_{ij} are implemented when the correct phase differences (0 or π) with no amplitude attenuation are introduced in the photon path states by the SLM.

Figure 2 shows two double-slit interference patterns, measured in coincidence counts. Both are obtained by scanning the signal beam detector, with steps of $40\ \mu\text{m}$, while maintaining the idler beam detector fixed in the position that corresponds to an interference pattern maximum ($x_i = 0$). In the closed squares pattern, we have used the same SLM gray level for the $|0\rangle$ and $|1\rangle$ signal photon path states. But in the open squares pattern we have inserted a relative phase between the photon states, through an appropriate choice of SLM gray levels for each one. Fitting the two interference graphs, we measure a relative phase of $\Delta\phi = 3.25 \pm 0.03$. To obtain the interference pattern in both detectors, we have used the L_i and L_{s1} lenses in our experimental configuration. It is important to note that the phase in the idler photon path states is not affected by the SLM gray level, because there is no polarizer in front of this detector [27].

In Fig. 3 we have the coincidence double-slit image,

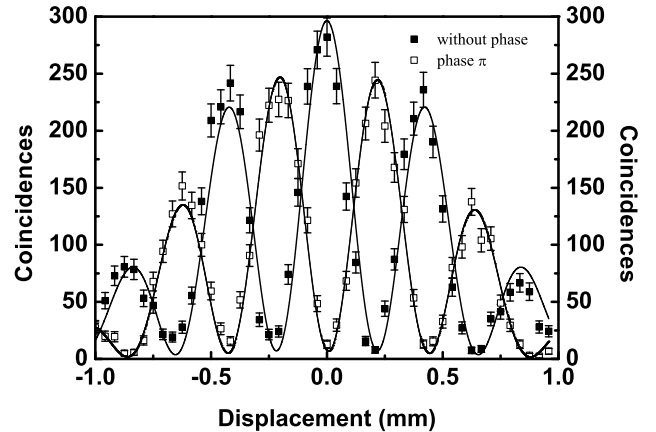


FIG. 2. Coincidence double-slit interference patterns. Closed squares show the interference pattern when the SLM gray levels are the same in both slit aperture directions that define the signal photon paths states. Open squares show the interference pattern when there are different gray levels producing a relative phase of π , between the signal states. Idler path phase, in both measurements, is not changed by the SLM. The idler detector is kept fixed at $x_i = 0$, while signal detector is scanned in steps of $40\ \mu\text{m}$ and the detection time is 60 seconds. Lenses L_i and L_{s1} were used.

for the signal beam. This result is obtained, when the L_{s2} lens is used in the signal beam and the L_i is used in the idler beam. Here the experimental setup is such that the peak in the x_s displacement negative region is associated with the inferior slit, i.e., with the $|0\rangle$ signal photonic state, while the peak in the positive displacement region is associated with the $|1\rangle$ photonic state. Once again we kept the idler detector fixed at $x_i = 0$, i.e., its interference pattern maximum and scan the signal beam detector, with steps of $20\ \mu\text{m}$ and acquisition time of $20\ \text{s}$. Signal detector is placed at the image plane while idler detector is at the Fourier plane. The SLM gray levels were the same as the ones used to obtain the open squares interference pattern shown in Fig. 2. We can infer that the SLM gray levels used to obtain phase π do not attenuate the state amplitude by calculating the areas under the peaks corresponding to each state. In the curve shown, we have an area of (77 ± 2) arb. units, for the $|0\rangle$ signal photon state and (72 ± 2) arb. units, for the $|1\rangle$ state. Therefore, with the curves shown in the open squares of Fig. 2 and Fig. 3, we can implement the U_{01} map. To implement each U_{ij} a proper gray level was chosen in each slit, corresponding to add a π phase for the value 1 and no extra phase for the value 0.

To implement the minimal Deutsch algorithm we must create the state $|+\rangle$ for the signal photon and, after the oracle, measure it in the base $\{|+\rangle, |-\rangle\}$. By detecting at the Fourier plane and at the origin of the interference pattern, we are able to implement experimen-

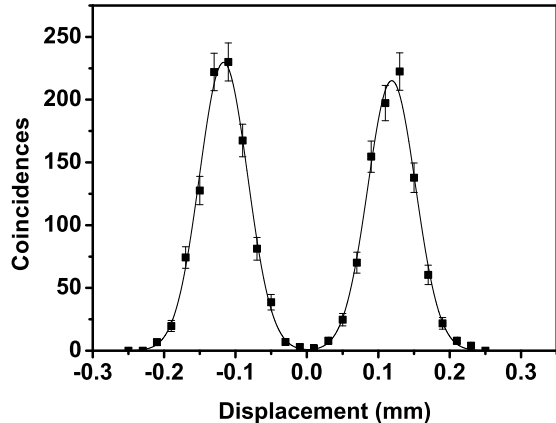


FIG. 3. Signal double-slit image, measured in coincidence counts. The result is recorded with the idler detector fixed at $x_i = 0$, while signal detector is scanned in the x direction, when the same gray level of open squares pattern used in Fig. 2 is applied and the detection time is 20 seconds. Lenses L_i (the same lens used in Fig. 2) and L_{s2} were used. Signal detector is placed at the image plane while idler detector is at the Fourier plane.

tally the detection projector $|+\rangle\langle+|$ [26]. Using SPDC, a double-slit, and by focusing the pump beam at the double-slit's plane, we prepare the Bell state $|\psi_{s,i}\rangle = |\psi^+\rangle = \frac{1}{\sqrt{2}}(|0_s 1_i\rangle + |1_s 0_i\rangle) = \frac{1}{\sqrt{2}}(|+_s +_i\rangle - |-_s -_i\rangle)$ [25]. If we detect the idler photon using the projection operator $|+\rangle\langle+|$ we project the signal photon state in the state we need. Hence, in our setting, an oracle query corresponds to a detection of the idler photon at the center of the pattern, being the instance where the logical qubit, the signal photon, is prepared in the appropriate state. The oracle's answer is then provided by the detection or no-detection of the signal photon. Note, moreover, that the idler measurement, and hence logical qubit state preparation, is done after one of the maps U_{ij} is applied on the qubit. But since these operations commute, this does not affect the final statistics.

The experimental results for all map possibilities are shown in Table I. The measured photon coincidences were obtained with signal and idler detectors kept fixed at $x_s = 0$, and $x_i = 0$ (center of the interference pattern), respectively, at the Fourier plane. Measurements were taken in 1000 s. The data show a clear difference of behavior between constant and balanced functions.

V. DISCUSSION

In the previous section we presented the result of the algorithm using many oracle queries, summarized in Table I, which allows, as expected, perfect discrimination between constant and balanced functions (high and low

TABLE I. Experimental results for all maps possibilities.

$f(0)$	$f(1)$	Coincidence
0	0	5218 ± 72
0	1	450 ± 21
1	0	427 ± 20
1	1	5399 ± 73

coincidence counts, respectively). The Deutsch algorithm is, however, about the optimization of the Deutsch problem with regard to the number of queries to the oracle; and here we discuss what our experimental setup tells us when only one such query is allowed.

However, the meaning of this implementation regarding individual events is more subtle, due, among other reasons, to the fact that an idler photon detection at position x corresponds to the preparation of a state $\frac{1}{\sqrt{2}}(|0\rangle + e^{i\phi(x)}|1\rangle)$ for the signal photon, where $\phi(x)$ is a function depending on the detector position and other features of the setting (see Refs.[25, 26]). Strictly speaking, the measurement is not of the von Neumann type, on the states $\{|+\rangle, |-\rangle\}$, but a positive operator valued measurement (POVM). This means that an infinitesimal detector in $x = 0$ measures an operator proportional to $|+\rangle\langle+|$, while a finite detector with opening d (that is, the width of the slit placed in front the detector) measures a positive operator that is a weighted sum of all projectors from $x = -\frac{d}{2}$ to $x = \frac{d}{2}$. Moreover, a signal no-detection event does not necessarily correspond to the state $|-\rangle$. Nevertheless, we can use the results shown in Fig. 2 to predict the chances of having a detection (and hence, also no detection) event when the function is constant or balanced, by computing the area under the corresponding (normalized) curve over an interval centered at the origin with the same width as the detector.

From the graphs themselves, and also from Table I, we see that the chances of detecting a photon when the function is constant is much higher than when it is balanced, so indeed a single oracle query gives us some information about the function. But, in practice, none of the events tell us *definitely* which type of function we have. A detection can also be associated with a balanced function, although it is rare, due to detector width. A no-detection event, on the other hand, might be related to one of three distinct situations: the function is balanced so, as we want, there is a very low probability of detecting a photon at the origin; or the function is constant, but the detector failed; the function is constant, but the photon hit the Fourier plane at another point away from the detector. Due to this third situation, even in a perfect experimental setting a no-detection event can also correspond to a constant function.

To understand better the quantum advantage within this implementation we can consider a scenario where one of these functions is given to us, with equal probability,

and we must bet on constant or balanced with only one oracle query. Classically, we cannot do better than a fifty-fifty guess, but with this implementation we can. Indeed, from the discussion in the last paragraph, we already see that a detection is more likely to be associated with a constant function, while no detection is more likely to be associated with a balanced one.

To see this in a quantitative manner, let S be the event where the function's type is correctly guessed. We can write the probability for this event as:

$$P(S) = \sum_{i,j=0,1} P(f = ij)P(S|f = ij), \quad (5)$$

where $P(f = ij) = 1/4$ is the probability of having the function $f(0) = i, f(1) = j$ while $P(S|f = ij)$ is the probability of success given that function. We denote by p_{ij} the probability for a photon to hit the Fourier plane at a point covered by the detector, given that the function implemented is $f = ij$. That is, p_{ij} is just the area under the normalized curve of Fig. 2 corresponding to the function ij , in an interval around the origin with the detector's width.

Now, if the function is the constant 00, we succeed in our guess if we detect a photon. This will take place with probability ηp_{00} , where η is the detector efficiency. Similarly, for $f = 11$, we have $P(S|f = 11) = \eta p_{11}$. For the function 01, on the other hand, we succeed if there is no detection, which has probability $(1 - p_{01}) + (1 - \eta)p_{01}$. The first term in the sum corresponds to the case where the photon goes to a point away from the detector, while in the second the photon hit the detector but the detector fails. Of course, we have also $P(S|f = 10) = (1 - p_{10}) + (1 - \eta)p_{10}$. Since the experiment is designed in a such a way that $p_{00} \approx p_{11} \equiv p_c$ and $p_{01} \approx p_{10} \equiv p_b$, we have finally:

$$P(S) = \frac{1}{2}[1 + \eta(p_c - p_b)]. \quad (6)$$

Of course, for any detector width, the probability is just $1/2$ for $\eta = 0$, since we do not gain any information about the function. It then grows linearly with η and, for the detector width we have used ($100\mu\text{m}$), it goes to a maximum of 0.55.

We could also vary the detector's size by changing the width of the slit placed in front of it, to maximize the right function choice. Figure 4 shows the success probability when the slit size is changed, and the detector is considered perfect. The best detector slit size is $260\mu\text{m}$ and the corresponding success probability is 0.58. For certain values the probability of detecting photons can be larger for balanced functions than for constant ones, so we would infer the function wrongly more often than correctly. Of course, we would then have to bet in the opposite way: balanced if we detect a photon, constant if we do not detect anything. For a detector covering the whole plane we recover the classical fifty-fifty guess since, again, we do not get any information about f .

We note finally that in this setting we have an asymmetry between the betting confidence on constant and balanced functions: For small detector sizes, a detection implies a constant function with high probability, while no detection implies a balanced one just with moderate probability. Indeed, from Bayes' formula we can compute:

$$P(f = \text{constant}|\text{detection}) = \frac{p_c}{p_c + p_b}, \quad (7)$$

$$P(f = \text{balanced}|\text{no-detection}) = \frac{1 - \eta p_b}{2 - \eta(p_c + p_b)}. \quad (8)$$

For instance, for a very small detector we have $p_b \ll p_c \ll 1$ so $P(f = \text{constant}|\text{detection}) \approx 1$ while $P(f = \text{balanced}|\text{no-detection}) \approx 1/2$. This is due to our choice of the detector position. Choosing a spot on the Fourier plane corresponding to the state $|-\rangle$ would invert this asymmetry. If a CCD was used instead we would have, on average, the same confidence for betting on both types of functions, but there would still be inconclusive events. If the signal photon were detected by the CCD on a position corresponding to the state preparation, say, $\frac{1}{\sqrt{2}}(|0\rangle + i|1\rangle)$, we could not infer the type of function we had. For instance, a detection at position 0.11mm , *i.e.*, where the two interference patterns cross in Fig. 2, corresponds to such a situation.

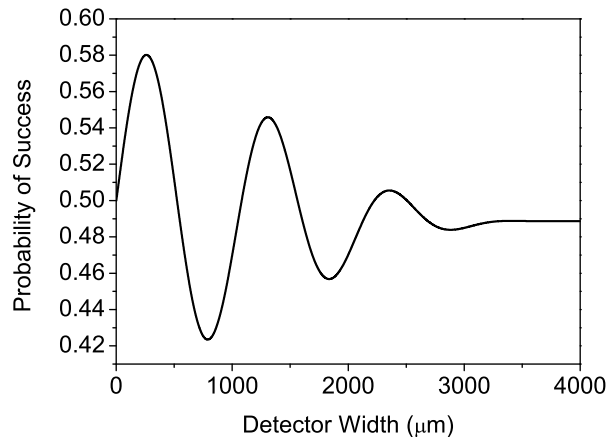


FIG. 4. Probability of success when the signal detector size is changed (width of the single slit in front of the detector is varied). The photon detectors are assumed to be fixed at the positions $x_i = x_s = 0$, and it is assumed the detection of the idler photon. Here the detectors are considered perfect, and we consider the average probability of both detection and no-detection events. It is assumed that we always bet in a constant (balanced) function when there is (no) detection. The optimal size for the detector is $260\mu\text{m}$, with a success probability of 0.58.

VI. CONCLUSIONS

In this work we implement the minimal Deutsch algorithm version with one qubit, using spontaneous parametric down conversion and idler photodetection as a heralded source of one photon and a spatial light modulator as the key part of the quantum oracle. A double-slit is used to encode a qubit in the photonic transversal spatial modes and the state is manipulated using the SLM. The experimental setup is able to implement all possible one bit constant and balanced functions easily. Furthermore, we discuss the improvement of this specific quantum experimental implementation, when compared to the analogous classical algorithm. This is the first quantum algorithm implemented using a SLM, opens the

possibility to implement more complex algorithms. For example, by changing the double-slit to an eight-slit interferometer [15], one can also implement the analogous minimal version of Deutsch-Jozsa algorithm for three-bit functions $f : \{0, 1\}^3 \rightarrow \{0, 1\}$.

ACKNOWLEDGMENTS

This work is part of the Brazilian National Institute for Science and Technology for Quantum Information and was supported by the Brazilian agencies CNPq, CAPES, and FAPEMIG. We acknowledge the *EnLight* group and P. L. de Assis, for very useful discussions.

-
- [1] D. Deutsch. *Proc. R. Soc. Lond. A*, 400:97–117, 1985.
 - [2] D. Collins, K. W. Kim, and W. C. Holton. *Phys. Rev. A*, 58:R1633, 1998.
 - [3] I. L. Chuang, L. M. K. Vandersypen, X. Zhou, D. W. Leung, and S. Lloyd. *Nature*, 393:143–146, 1998.
 - [4] L. M. K. Vandersypen, M. Steffen, G. Breyta, C. S. Yannoni, M. H. Sherwood, and I. L. Chuang. *Nature*, 414:883–887, 2001.
 - [5] S. Gulde, M. Riebe, G. P. T. Lancaster, C. Becher, J. Eschner, H. Haffner, F. Schmidt-Kaler, I. L. Chuang, and R. Blatt. *Nature*, 410:44–50, 2003.
 - [6] V. Giovannetti, D. Vitali, and P. Tombesi. *Optics and Spectroscopy*, 91:423–428, 2001.
 - [7] J. Siewert and R. Fazio. *Journal of Modern Optics*, 49:1245–1254, 2002.
 - [8] P. Walther, K. J. Resch, T. Rudolph, E. Schenck, H. Weinfurter, V. Vedral, M. Aspelmeyer, and A. Zeilinger. *Nature*, 434:169–176, 2005.
 - [9] G. Vallone, G. Donati, N. Bruno, A. Chiuri, and P. Mataloni. *Phys. Rev. A*, 81:R050302, 2010.
 - [10] D. Deutsch and R. Jozsa. *Proceedings: Mathematical and Physical Sciences*, 439(1907):553–558, 1992.
 - [11] A. N. Oliveira, S. P. Walborn, and C.H. Monken. *Journal of Optics B: Quantum and Semiclassical Optics*, 7:288, 2005.
 - [12] P. Bianucci, A. Muller, C.K. Shih, Q.Q. Wang, Q.K. Xue, and C. Piermaroc. In *International Quantum Electronics Conference*. Optical Society of America, 2004.
 - [13] Z. Y. Ou and L. Mandel. *Phys. Rev. Lett.*, 61:50–53, 1988.
 - [14] Y. H. Shih and C. O. Alley. *Phys. Rev. Lett.*, 61:2921–2924, 1988.
 - [15] L. Neves, G. Lima, J. G. Aguirre Gómez, C. H. Monken, C. Saavedra, and S. Pádua. *Phys. Rev. Lett.*, 94:100501, 2005.
 - [16] J. G. Rarity and P. R. Tapster. *Phys. Rev. Lett.*, 64:2495–2498, 1990.
 - [17] A. Rossi, G. Vallone, A. Chiuri, F. De Martini, and P. Mataloni. *Phys. Rev. Lett.*, 102:153902, 2009.
 - [18] A. Mair, A. Vaziri, G. Weihs, and A. Zeilinger. *Nature*, 412:313–316, 2001.
 - [19] N. K. Langford, R. B. Dalton, M. D. Harvey, J. L. O’Brien, G. J. Pryde, A. Gilchrist, S. D. Bartlett, and A. G. White. *Phys. Rev. Lett.*, 93:053601, 2004.
 - [20] G. Lima, A. Vargas, L. Neves, R. Guzmán, and C. Saavedra. *Optics Express*, 17(13):10688–10696, 2009.
 - [21] S. Cialdi, D. Brivio, and M. G. A. Paris. *Phys. Rev. A*, 81:042322, 2010.
 - [22] W. M. Pimenta, B. Marques, M. A.D. Carvalho, M. R. Barros, J. G. Fonseca, J. Ferraz, M. Terra Cunha, and S Pádua. *Optics Express*, 18:24423–24433, 2010.
 - [23] J. Leach, B. Jack, J. Romero, M. Ritsch-Marte, R. W. Boyd, A. K. Jha, S. M. Barnett, S. Franke-Arnold, and M. J. Padgett. *Optics Express*, 17:8287–8293, 2009.
 - [24] G. Puentes, C. La Mela, S. Ledesma, C. Iemmi, J. P. Paz, and M. Saraceno. *Phys. Rev. A*, 69:042319, 2004.
 - [25] L. Neves, S. Pádua, and C. Saavedra. *Phys. Rev. A*, 69:042305, 2004.
 - [26] L. Neves, G. Lima, E. J. S. Fonseca, L. Davidovich, and S. Pádua. *Physical Review A*, 76(3):032314, 2007.
 - [27] I. Moreno, P. Velásquez, C. R. Fernández-Pousa, and M. M. Sánchez-López. *J. App. Phys.*, 94:3697, 2003.